Three-Dimensional THz Imaging

Final Report

submitted to Dr. Gernot Pomrenke

Physics Division

US Air Force Office of Scientific Research

April 20, 2005

Principal Investigator:

Prof. Theodore B. Norris

Center for Ultrafast Optical Science

EECS Department, University of Michigan

2200 Bonisteel Blvd, Ann Arbor, MI 48109-2099

(734) 764-9269

Abstract

Three-dimensional imaging has been demonstrated using single-cycle terahertz electromagnetic pulses. Reflection-mode imaging was performed with a photoconductive transmitter and receiver and a reconstruction algorithm based on time reversal. A two-dimensional array was synthesized from ten concentric ring annular arrays with numerical apertures ranging from 0.27 to 0.43. The system clearly distinguished image planes separated by 1.5 mm and achieved a lateral resolution of 1.1 mm. In terms of the illuminating terahertz power spectrum, the lateral resolution was 38% and 81% of the peak and mean wavelengths, respectively. Coded excitation has also been explored to improve the signal-to-noise ratio. A separate imaging system was constructed, where a 53-bit binary waveform is transmitted while the received signals are digitally compressed. Two-dimensional objects have been imaged with a 13 dB improvement in signal-to-noise ratio.

I. Research Summary

(1) List of Manuscripts

T. Buma and T.B. Norris, "Coded excitation of broadband terahertz using optical rectification in poled lithium niobate," submitted to Applied Physics Letters.

T. Buma and T.B. Norris, "Coded excitation of broadband terahertz using optical rectification in poled lithium niobate," paper CThX7, to be presented at CLEO (2005).

T. Buma and T.B. Norris, "Time reversal 3-D imaging using single-cycle terahertz pulses," Appl. Phys. Lett., vol. 84, 2196 (2004).

T. Buma and T.B. Norris, "Time-Reversal 3-D Imaging Using Single-Cycle THz Pulses," paper CMP4, presented at CLEO (2003).

(2) Scientific Personnel Supported

1. Tak Buma, postdoctoral research associate
2. T.B. Norris, principal investigator

(3) Inventions

No patents applied for.

(4) Scientific Progress and Accomplishments

Photoconductive terahertz (THz) emitter and receiver units from Picometrix were used to construct a synthetic aperture system for imaging three-dimensional objects. We have also explored coded excitation to improve the signal-to-noise ratio (SNR) of THz imaging, a major issue for practical applications. Instead of using the photoconductive units, we have constructed a separate imaging system relying on non-linear optical crystals. The encoded transmitter is based on optical rectification in poled lithium niobate, while electro-optic detection is performed in zinc telluride.

Experimental Program: Three-dimensional imaging

There is presently considerable interest in using single-cycle terahertz electromagnetic pulses for imaging[1-6]. Terahertz waves can penetrate a variety of optically opaque plastics and ceramics. The large bandwidths and sub-millimeter wavelengths are attractive for spectroscopic imaging. A promising imaging technique is time reversal imaging[1,2], which has successfully reconstructed 1-D and 2-D objects. In this study we have extended the technique to 3-D imaging.

Time reversal imaging is a coherent imaging technique. As shown in Fig. 1(a), a transmitted pulse is incident on the object of interest, where the scattered fields are detected by an array of receivers. An image point is reconstructed in a two-step process. First, the time delays are computed for a terahertz pulse to propagate from the transmitter to the image point, and then from the image point to each receiver. Second, the received signal samples corresponding to the computed time delays are summed together to produce the amplitude of the image point. The propagation distances also determine the amplitude weighting of each sample during the summation. It must be emphasized that all the image points are reconstructed using the same received data. Each image point requires a different set of time delays and therefore a different summation of the receiver signals. This "delay-sum" algorithm, commonly used in medical ultrasound imaging[7], is

entirely equivalent to back-propagating the received signals using the time reversed Huygens-Fresnel diffraction integral[1,2] (see Fig. 1(b)).

The imaging setup is shown in Fig. 2. The heart of the system consists of the fiber-coupled photoconductive transmitter and receiver modules[10]. The fiber-coupling permits arbitrary placement of the modules for synthetic aperture imaging. The modules are driven by a homemade 76 MHz Ti:sapphire oscillator. The 80 fs oscillator pulses are first sent through a double-pass grating stretcher to compensate the dispersion in the 1 m long single-mode fibers of each module. A half-wave plate and polarizing beamsplitter divide the pre-chirped pulses into a transmitter arm and receiver arm. The receiver pulses are sent through a rapid-scanning delay line before entering the receiver module fiber. The delay line scans a 120 ps window at a rate of 5 Hz. The signal from the receiver is sent directly to an A/D board without using lock-in detection.

The object consists of aluminum foil letters spelling "CUOS" attached to a high-density polyethylene substrate, as shown in Fig. 3(a). Each letter is approximately 12 mm tall and 3 mm wide with a linewidth of 1 mm. 1.5 mm deep steps machined into the substrate place each letter at a different z-coordinate. The object is approximately centered on the z-axis.

Ideally, an array of transmitters and receivers are used to perform terahertz imaging. The unavailability of such an array forces us to rely on synthetic aperture techniques. A single transmitter and receiver are used to synthesize a highly populated array by firing the transmitter multiple times while rotating the object between firings. This is equivalent to mechanically scanning the transmitter and receiver between firings. Once all the signals have been collected, the image reconstruction algorithm treats the data set as if it were acquired by an actual array.

A ring annular array is synthesized by rotating the object along the z-axis while the transmitter and receiver remain stationary[1]. The transmitter and receiver are located 142 mm and 102 mm, respectively, from the origin of the imaging system. The off-axis angle of the transmitter is $\theta_T = 26.5^\circ$. A 90-element array is synthesized by rotating the object in 4° increments after every 100 signal averages. The numerical aperture (NA) of the array is determined by $NA = \sin\theta_T - \sin\theta_R$.

Changing θ_R after each full rotation of the object produces a set of concentric ring annular arrays. Ten concentric rings were synthesized by varying θ_R from 1 to10° in1° increments. As shown in Fig. 3(b), the multiple rings combine to form an annular imaging aperture with an "inner" NA of 0.27 and an "outer" NA of 0.43. A reconstructed image is a weighted sum of the images reconstructed from each ring aperture. The weighting is based on approximating the area of the annulus by summing the areas of each ring. Since the rings are distributed along a sphere, the area of a ring is proportional to its NA.

The reconstructed image planes containing the letters "C", "U", "O", and "S" are shown in Fig. 4(a)-(d), respectively. Each image covers a 25 x 25 mm field of view. All images are displayed over the same linear gray scale where white (black) represents positive (negative) field amplitude and mid-gray corresponds to zero. Each letter is clearly reconstructed, demonstrating the ability to distinguish image planes along the z-axis. The fainter "C" and "S" are due to the limited spot size of the Gaussian-shaped illuminating terahertz beam. Line-outs taken along Fig. 4(a)-(d) reveal -6dB widths of 1.3, 0.8, 0.9, and 1.2 mm, respectively. Reconstructing image points farther away from the origin is more sensitive to slight errors in alignment of the transmitter and receiver modules. The average lateral resolution is 1.1 mm, corresponding to 38% and 81% of the peak and mean wavelengths, respectively, of the illuminating terahertz power spectrum.

In every image of Fig. 4, faint patches of white and black are visible in regions away from a letter. These artifacts are shown more vividly by the images reconstructed from a single ring rather than the weighted sum of all the rings. Fig. 5(a)-(d) show reconstructed images of the letter "U" from single rings with NA = 0.43, 0.38, 0.32, and 0.27, respectively. The most striking features are the bright arcs sweeping across the images. When combining images from multiple rings, these artifacts fail to reinforce each other since their positions are different in each image. In contrast, the reconstructed letters reinforce each other since their positions in the images remain the same. As a result, the annular array images in Fig. 4 have weaker artifacts than the single-ring images of Fig. 5.

The origin of these artifacts can be understood by analyzing the point spread function (PSF) of a single ring array. The analysis is simplified by assuming the array as continuously sampled around its circumference. The paraxial approximation is applied to

the time-reversed Huygens-Fresnel diffraction integral[1], which is commonly made in the analysis of ultrasonic transducer arrays[11]. A point object is placed at the origin of the system. Expressed in cylindrical coordinates, the reconstructed image field is given by:

$$u(r,z) = \int_{-\infty}^{\infty} \frac{d\omega}{2\pi} \kappa_0 \, \omega^2 u_{in}(\omega) J_0(\omega \, NA \, r / c) \exp(-i\omega z \zeta / c) \qquad (1)$$

where $\zeta = \cos\theta_T + \cos\theta_R$ and c is the speed of light in air. The term κ_0 is a geometrical factor depending on the synthetic array dimensions, while $u_{in}(\omega)$ is the frequency spectrum of the terahertz field incident on the point target. When r is much larger than the peak wavelength of the terahertz spectrum, the Bessel function J_0 in (1) can be replaced by its large argument expansion to give:

$$u(r,z) = \int_{-\infty}^{\infty} \frac{d\omega}{2\pi} \kappa_0 \, \omega^2 u_{in}(\omega) \frac{\cos(\omega \, NA \, r / c - \pi / 4)}{\sqrt{2\pi\omega \, NA \, r / c}} \exp(-i\omega z \zeta / c) \qquad (2)$$

Applying the principle of stationary phase, the major contribution to the integral in (2) occurs when $r = |z| \, \zeta / \mathrm{NA}$. This produces a ring-shaped halo in the reconstructed image of a plane located a distance $|z|$ from the point object. The halo radius varies with the numerical aperture of the array.

We performed simulations to visualize this halo artifact. The model consists of a 0.47 NA ring annular array imaging a point scatterer at the origin. All gray scale images cover a 12.5 x 12.5 mm area. The reconstructed image of the x-y plane containing the point object is shown in Fig. 6(c). This is what one intuitively expects for the lateral PSF. The reconstructed image of the x-y plane 1 mm in front of the point object (z = -1 mm) is shown in Fig. 6(d). The circular feature is the previously described halo. This helps explain the artifacts in Fig. 4; the bright arcs are from letters in other object planes. In other words, the reconstructed image is corrupted by scattered waves from out-of-plane

objects. Consequently, 3-D imaging is not simply a matter of using a single-ring annular array[1] to reconstruct multiple depths.

The strength of the halo artifact is measured by computing the image intensity along the dashed line in Fig. 6(d). This is repeated for all image planes distributed within -6.25 $< z <$ 6.25 mm. The intensity function is then integrated over z and displayed by the solid curve in Fig. 7. The central lobe reveals the lateral resolution of the system, while the slowly decaying pedestal indicates the strength of artifacts. The dotted curve shows the simulated beam plot of the ten-ring aperture used in the experiment. The much lower pedestal reveals that artifacts are indeed suppressed by using a more highly filled 2-D aperture. An even lower pedestal is shown by the dashed curve, which simulates a completely filled disk aperture synthesized from 26 rings. The central lobe is slightly wider since the smaller diameter rings contribute lower spatial frequencies. However, the dramatic suppression in artifacts far outweighs the slight broadening of the lateral PSF.

In summary, we have demonstrated time reversal 3-D imaging using single-cycle terahertz electromagnetic pulses. The system clearly distinguishes image planes separated by 1.5 mm and achieves a -6 dB lateral resolution 38% and 81% of the peak and mean terahertz wavelengths, respectively. 3-D reconstruction artifacts are excessively high using a single-ring annular array. As a result, a more highly filled 2-D aperture is necessary to suppress the artifacts.

Experimental Program: Coded excitation

A major limitation to THz imaging is signal-to-noise ratio (SNR), especially when imaging weakly scattering objects. Obviously, SNR can be improved with more efficient transmitters. An alternative method for improving SNR is coded excitation, a well established technique in radar[11] and ultrasound imaging[12]. Coded excitation is particularly useful when there are peak power limitations on the transmitter (e.g., peak-power damage in nonlinear crystals). The transmitted pulse is an encoded waveform with a long duration but large bandwidth, as shown in Fig. 8(a). The received waveforms are digitized and decoded by a discrete-time filter. This decoding filter digitally compresses the encoded waveforms to produce short pulses with high peak power, as shown in Fig.

8(b). The SNR improvement scales with the time-bandwidth product of the transmitted waveforms.

Coded excitation can be used with a variety of encoding waveforms. Binary phase codes are particularly attractive for systems with limited capabilities for amplitude and frequency modulation. These codes consist of the same pulse repeated at regular intervals, where the sign of the pulse is either +1 or –1. The bandwidth of the overall code is determined by the bandwidth of an individual pulse. Binary phase codes of electromagnetic THz waveforms can be generated by optical rectification in poled lithium niobate (PLN). PLN crystals have been shown to generate simple narrow-band THz as well as more complicated waveforms[13]. This is possible by engineering the poling domain structure of the crystal. Roughly speaking, each poling domain contributes a half-cycle of THz field. The phase of a particular half-cycle is determined by the poling direction of its source domain. Assigning a binary code to the crystal poling pattern therefore produces a binary phase encoded THz waveform.

The experimental setup is illustrated in Fig. 9. The ultrafast laser is a home-built 250 kHz regeneratively amplified Ti:Sapphire system. The pump beam is chopped at 65 kHz before it is focused onto the PLN crystal with a 40 cm focal length lens. The pump pulse energy is approximately 600 nJ. The generated THz is collimated and re-focused by two metallic off-axis parabolas. THz detection is performed with a standard electro-optic setup. The probe laser is first sent through a rapid scanning delay line covering a 140 ps window at a repetition rate of 2.5 Hz. The probe pulse energy is approximately 60 nJ. The probe beam then passes through a Glan-Thompson polarizer and reflects off a pellicle to co-propagate with the THz. The THz-induced birefringence inside the ZnTe sensor crystal modulates the polarization of the probe laser. A quarter-wave plate followed by a Wollaston prism produces two optical beams for balanced detection. The balanced signal is fed through a lock-in amplifier (30 μs time constant) and digitized by a 16-bit A/D board at a sampling rate of 100 kS/s.

The PLN crystal, custom manufactured by Deltronic Crystal Industries, is 5 mm long and 0.5 mm thick. The poling pattern consists of a 53-bit binary code[14]. As shown by the inset of Fig. 9, each bit consists of a pair of domains with opposite poling directions. The length of each bit is L_b = 94 μm, so each poling domain is 47 μm long. The peak THz

frequency is expected to be $f_{peak}=c/(n_T-n_o)L_b$[15], where n_T and n_o are the THz and optical indices of refraction, respectively. Assuming $n_T = 5.2$ and $n_o = 2.3$ produces $f_{peak} = 1.1$ THz. Since lithium niobate has significant THz absorption at room temperature[15], the PLN crystal was cooled in a liquid helium cryostat. The exit window of the cryostat is made of high-density polyethylene, blocking the residual optical beam while transmitting most of the generated THz.

The first experiment was a straight "pitch-catch" measurement, where no object was placed in the THz beam path. A single-shot measurement of the encoded waveform is shown in Fig. 10(a). The x-axis is time in ps and the y-axis is the normalized signal amplitude. This signal was digitally bandpass filtered between 0.5 and 2.2 THz to suppress out-of-band noise. Digital pulse compression was performed with an inverse filter in the frequency domain[12]. This filter was derived empirically from a separate "pitch-catch" measurement involving 1000 signal averages. The inverse filter was obtained by inverting the spectrum of this averaged signal. Theoretically, the 53-bit binary code patterned into the PLN crystal has a well behaved spectrum suitable for spectrum inversion[12]. The raw (no bandpass filtering) signal used to produce Fig. 10(a) was then digitally compressed to produce Fig. 10(b). Clearly a tight pulse is produced, along with a reduction in the noise level. The digital pulse compression is a form of signal averaging, since the individual pulses in the binary code are effectively "re-aligned" and added together. The spectra of the compressed and encoded signals are shown by the solid and dashed curves in Fig. 10(c), respectively. The x-axis is frequency in THz while the y-axis is normalized magnitude in dB. The ripples in the encoded signal spectrum are due to interference between the temporally separated pulses (the "bits") of the binary waveform. The digital compression filter removes most of the ripples in the encoded signal spectrum to produce a much smoother spectrum peaked at 1.2 THz with a –6 dB bandwidth of 1.2 THz.

The pulse compression filter was tested with a simple one-dimensional imaging experiment, where an object was placed in the THz beam path. The object consists of a 6 mm thick high-density polyethylene plate. A 3 mm deep step is machined into this plate, as shown in Fig. 9. Placing this object approximately two-thirds into the THz beam path produces three pulses arriving at the THz detector. The first pulse is due to the THz

propagating purely in air. The second and third pulses are due to the THz transmitted through the thin and thick sections of the object, respectively. A single-shot waveform followed by bandpass filtering is shown in Fig. 11(a). The x-axis is time in ps and the y-axis is normalized amplitude. The same filter used to produce Fig. 11(b) was applied to the raw (no bandpass filtering) single-shot waveform. The digitally compressed signal is shown in Fig. 11(b), clearly showing the three pulses expected from the object. For comparison, the poled PLN crystal was replaced with a 1mm thick ZnTe crystal. The single-shot waveform, followed by bandpass filtering, is shown in Fig. 11(c). The residual signal trailing the three main pulses is a common occurrence in terahertz exp eriments with ZnTe crystals. This is most likely due to reverberations and terahertz absorption lines in the ZnTe[16]. The coded excitation scheme clearly shows comparable performance to the ZnTe emitter.

This same coded excitation scheme was further evaluated with a two-dimensional imaging experiment. The setup is shown in Fig. 12, which is similar to Fig. 9. The main difference is the two metal-coated mirrors in between the off-axis parabolas. The first mirror directs the encoded terahertz onto the object, while the second mirror directs a portion of the scattered THz onto the second parabola for detection. As shown in Fig. 13(a), the object consists of two steel drill bits spaced 5 mm apart. An array is synthesized by rotating the object while the transmitter and receiver remain fixed. The effective transceiver aperture is depicted in Fig. 13(b).

A typical waveform from the acquired data set is shown in Fig. 14(a). All signals were averaged sixteen times before storage. The average SNR of the signals is computed to be 7.5 dB. Applying a pulse compression filter produces the waveform in Fig. 14(b), producing two clearly identifiable pulses. The average SNR of the compressed signals is computed to be 20.5 dB, representing an improvement of 13 dB. This same compression filter was applied to all the acquired signals before performing image reconstruction. The final image is shown in Fig. 14(c), clearly showing the two objects.

Ideally, the pulse compression filter performs signal averaging by re-aligning the individual pulses and adding them together. This would produce an SNR improvement of $10\log_{10}(N)$, where N is the number of bits in the code. However, any inverse filter possesses a noise figure, resulting in a slight degradation of SNR. Theoretically, the SNR

penalty is only 0.5 dB for the 53-bit code used in these experiments[14]. The ideal SNR improvement for a 53-bit code should therefore be $10\log_{10}(53) - 0.5 = 16.75$ dB. The discrepancy between the ideal and observed SNR improvement can be attributed to a couple of factors. The digital compression filter used in this study was computed heuristically and is by no means an optimal filter. The transmitted binary code can be degraded by slight imperfections in the poling of the lithium niobate crystal. Even with a perfectly poled crystal, the transmitted code has distortions due to terahertz diffraction within the crystal. This means different segments of the transmitted code will not be perfectly collimated by the first off-axis parabola. A larger optical pump beam can reduce these effects, but the lower intensity will considerably weaken the optical rectification. Furthermore, practical implementations of digital filters operate in the time domain instead of the frequency domain. Time-domain filters will require optimization methods to simultaneously improve SNR while suppressing range sidelobes that naturally occur in the pulse compression process[17].

In summary, coded excitation of broadband terahertz has been performed using optical rectification in poled lithium niobate patterned with a 53-bit binary phase code. Digital pulse compression produces near single-cycle terahertz pulses at 1.2 THz. Initial one-dimensional imaging experiments show that the coded excitation scheme compares favorably with a conventional ZnTe emitter. This system has imaged two-dimensional objects with a 13 dB improvement in SNR.

REFERENCES

[1]A. B. Ruffin, J. V. Rudd, J. Decker, L. Sanchez-Palencia, L. Lehors, J. F. Whitaker, and T. B. Norris, IEEE J. Quantum Electron., **38**, 1110 (2002).

[2]A. B. Ruffin, J. Decker, L. Sanchez-Palencia, L. Lehors, J. F. Whitaker, T. B. Norris, and J. V. Rudd, Opt. Lett., **26**, 681 (2001).

[3]B. Ferguson, S. Wang, D. Gray, D. Abbot, and X. C. Zhang, Opt. Lett., **27**, 1312 (2002).

[4]J. O'Hara and D. Grischkowsky, Opt. Lett., **27**, 1070 (2002).

[5]T. D. Dorney, J. L. Johnson, J. V. Rudd, R. G. Baraniuk, W. W. Symes, and D. M. Mittleman, Opt. Lett., **26**, 1513 (2001).

[6]K. McClatchey, M. T. Reiten, and R. A. Cheville, Appl. Phys. Lett., **79**, 4485 (2001).

[7]A. Macovski, *Medical Imaging Systems* (Prentice Hall, Englewood Cliffs, NJ, 1983).

[8]D. L. Mensa, *High Resolution Radar Cross-Section Imaging* (Artech House, Norwood, MA, 1991).

[9]T. Melamed, Y. Ehrlich, and E. Heyman, Inverse Probl., **12**, 977 (1996).

[10]PT2001TX and PT2001RX, Picometrix, Inc., Ann Arbor, MI.

[11]M. I. Skolnik, *Radar Handbook, 2nd ed.* (McGraw-Hill, New York, NY 1980).

[12]Y. Wang, K. Metzger, D. N. Stephens, G. Williams, S. Brownlie, and M. O'Donnell, "Coded excitation with spectrum inversion (CEXSI) for ultrasound array imaging," IEEE Trans. Ultrason., Ferroelect., Freq. Contr., **50**, 805-823 (2003).

[13]Y.-S. Lee, N. Amer, and W. C. Hurlbut, "Terahertz pulse shaping via optical rectification in poled lithium niobate," Appl. Phys. Lett., **82**, 170-172 (2003).

[14]J. Ruprecht and M. Rupf, "On the search for good aperiodic binary invertible sequences," IEEE Trans. Inform. Theory, **42**, 1604-1612 (1996).

[15]Y. S. Lee, T. Meade, T. B. Norris, and A. Galvanauskas, "Tunable narrow-band terahertz generation from periodically poled lithium niobate," Appl. Phys. Lett., **78**, 3583-3585 (2001).

[16]M. Schall, M. Walther, and P. Uhd Jepsen, Fundamental and second-order phonon processes in CdTe and ZnTe," Phys. Rev. B, **64**, 094301 (2001).

[17]M. O'Donnell, "Coded excitation system for improving the penetration of real-time phased-array imaging systems," IEEE Trans. Ultrason., Ferroelect., Freq. Contr., **39**, 341-351 (1992).

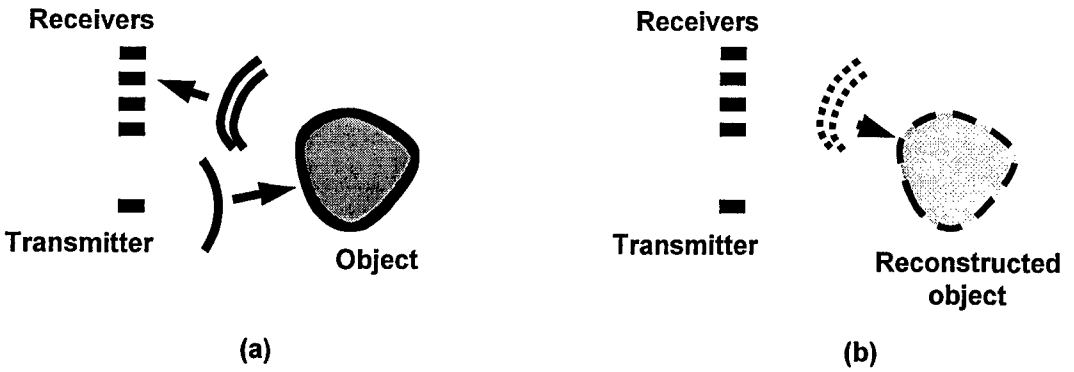

Fig. 1: Basic procedure for terahertz imaging. (a) Data acquisition (b) Image reconstruction.

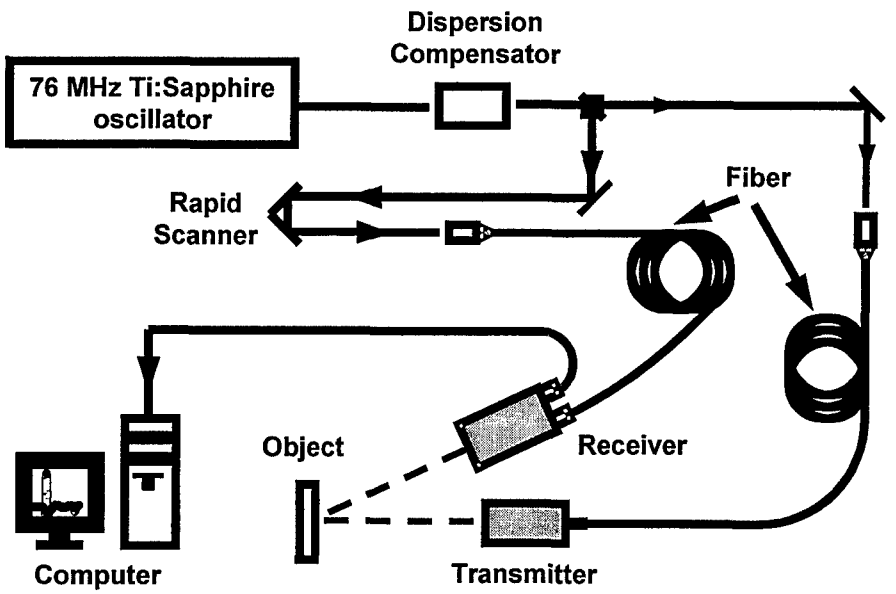

Fig. 2: Experimental setup for terahertz imaging with single-cycle pulses.

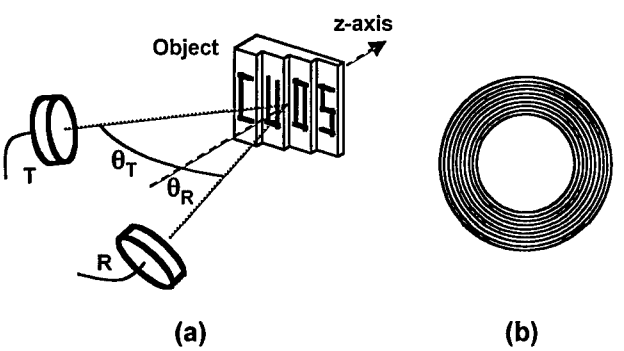

Fig. 3: (a) Geometry for reflection-mode imaging. (b) Effective transceiver aperture.

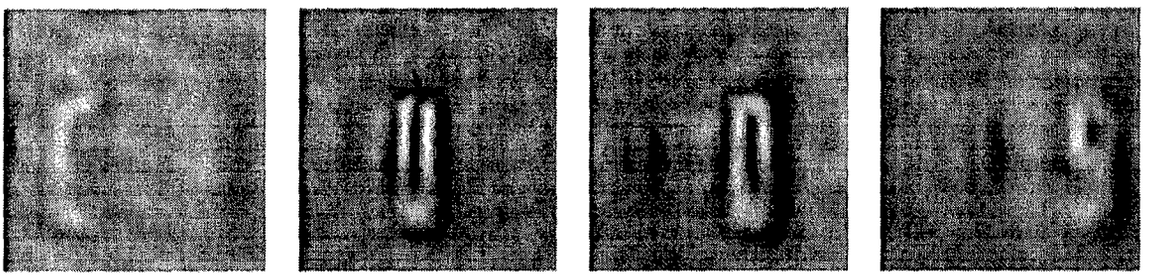

Fig. 4: Reconstructed image planes for (a) "C", (b) "U", (c) "O", and (d) "S".

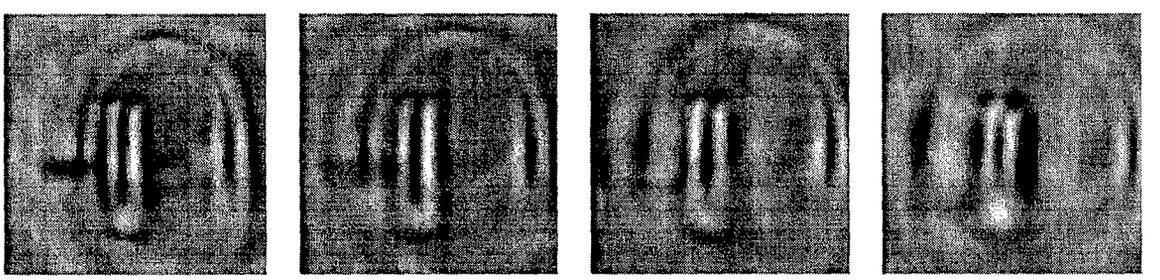

Fig. 5: Reconstructed images of the letter "U" using a single ring with (a) NA = 0.43, (b) NA = 0.38, (c) NA = 0.32, and (d) NA = 0.27.

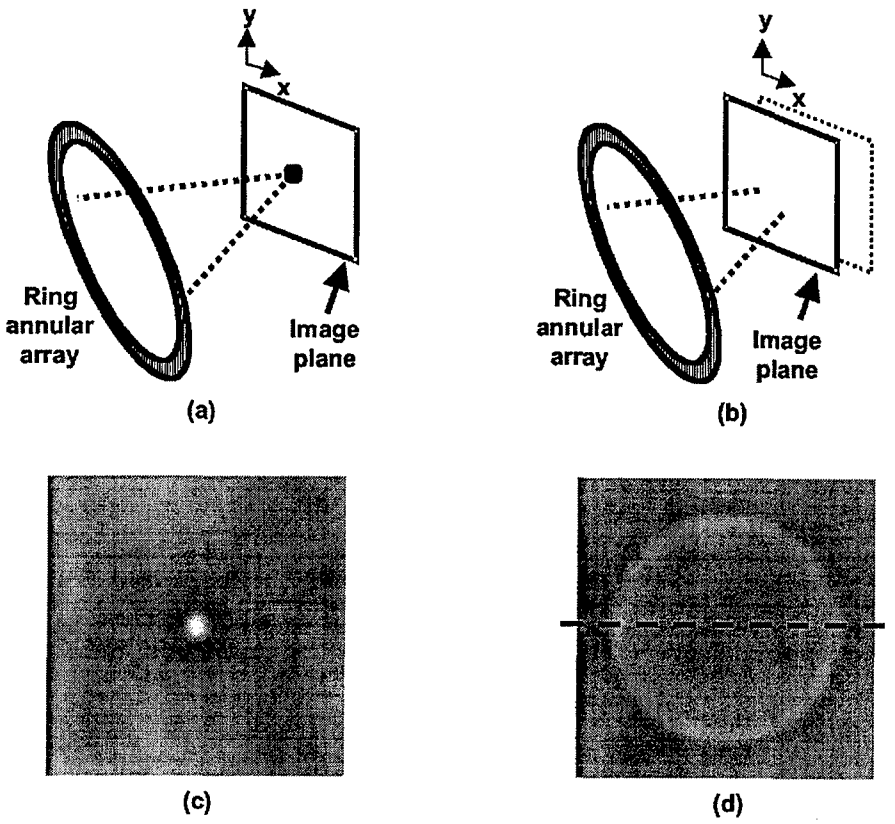

Fig. 6: Geometry for simulated point spread function (PSF) of a single ring-annular array. (a) Image plane containing the point object. (b) Image plane 1mm in front of the object. (c) Reconstructed PSF of the image plane in (a). (d) Reconstructed image of the plane shown in (b).

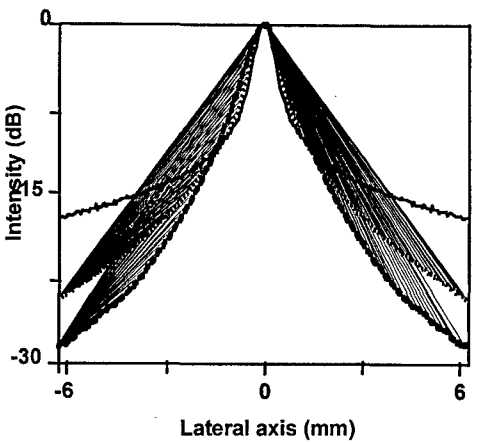

Fig. 7: Beam plots for an effective transceiver aperture consisting of 1 ring (solid curve), 10 rings (dotted curve), and 26 rings (dashed curve). More highly filled 2-D apertures suppress artifacts.

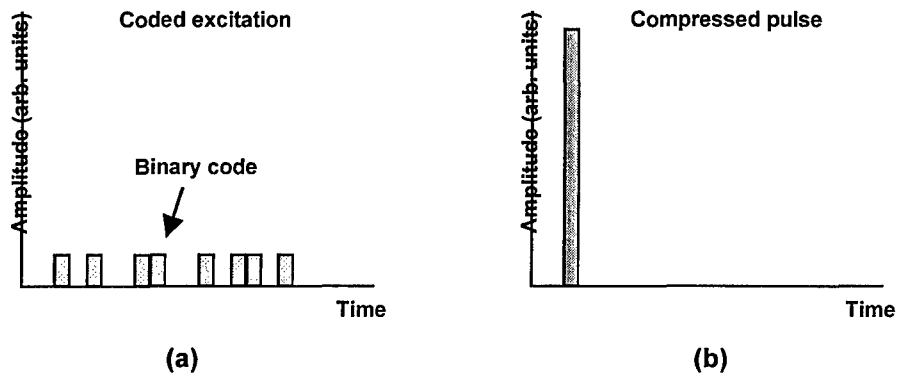

Fig. 8: Basic concept behind coded excitation. (a) Transmit a long encoded sequence. (b) Apply a digital filter to compress the received waveform into a single large pulse.

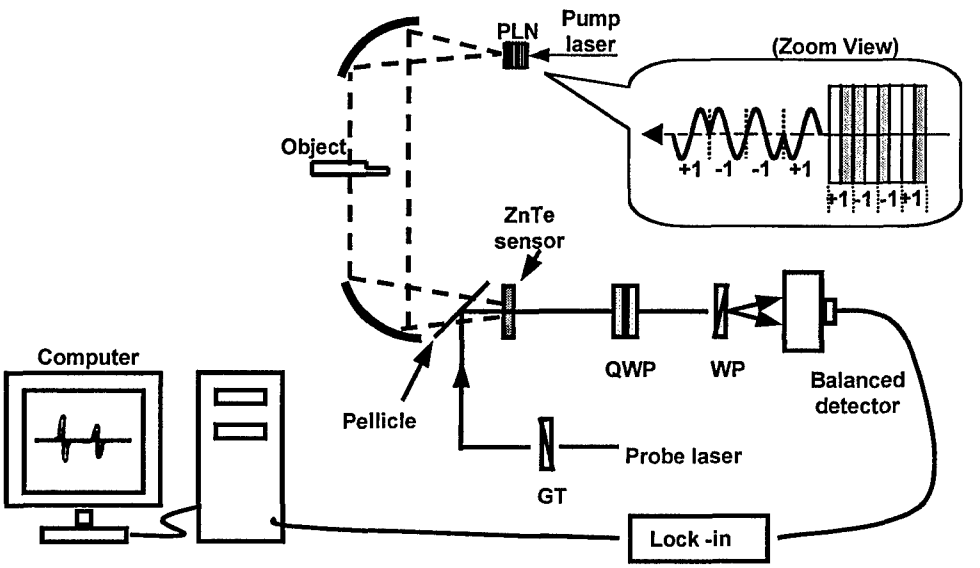

Fig. 9: Experimental setup for coded excitation of broadband terahertz.

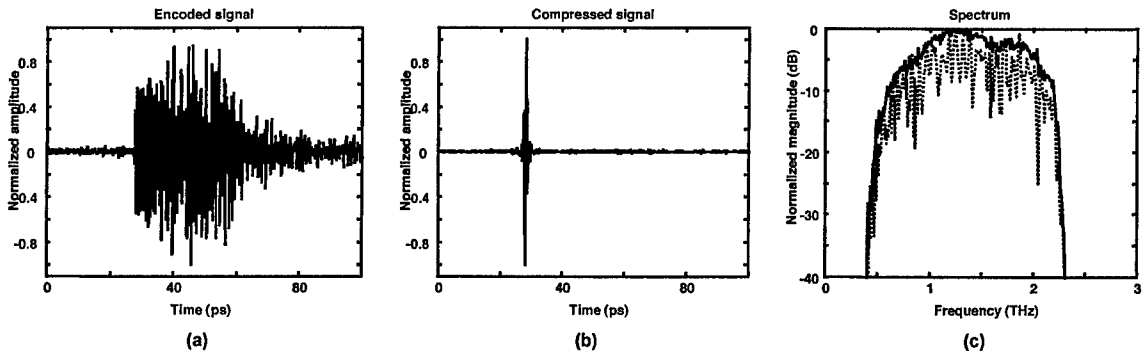

Fig. 10: Coded excitation results with no object in the THz path. (a) Encoded waveform. (b) Digitally compressed signal. (c) Spectra of the two signals. The encoded and decoded spectra are shown by the dotted and solid curves, respectively.

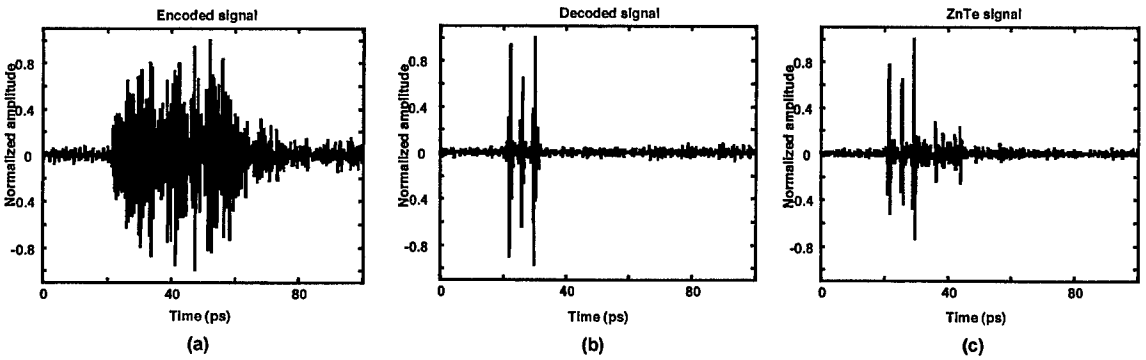

Fig. 11: Coded excitation results with the object in the THz path. (a) Encoded waveform. (b) Digitally compressed signal. (c) Signal acquired with a ZnTe emitter.

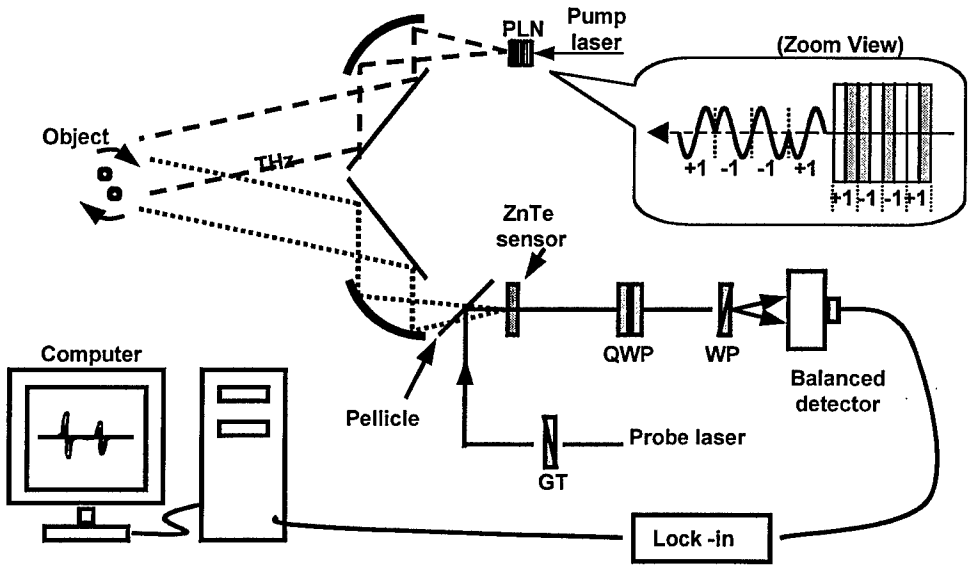

Fig. 12: Experimental layout for 2-D imaging with coded excitation.

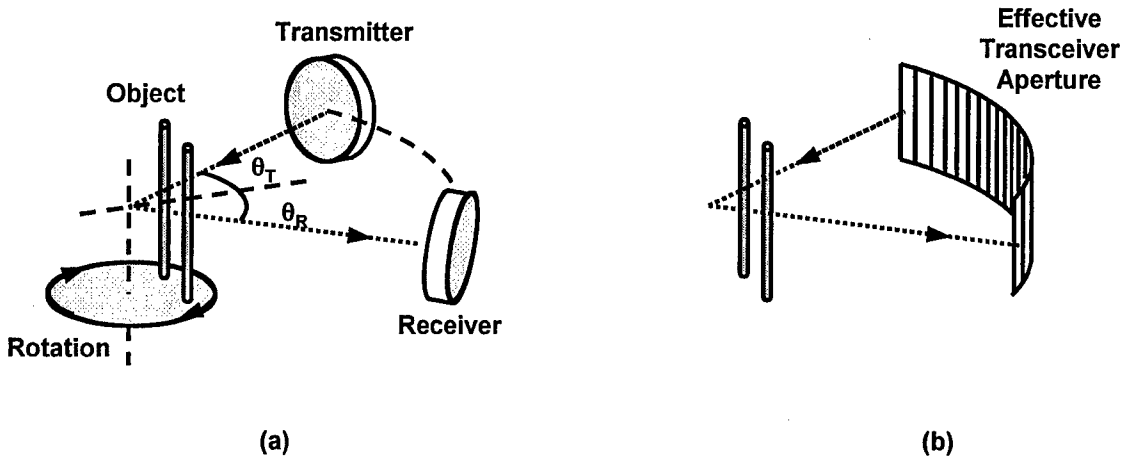

Fig. 13: (a) Geometry for two-dimensional imaging. (b) Effective transceiver aperture.

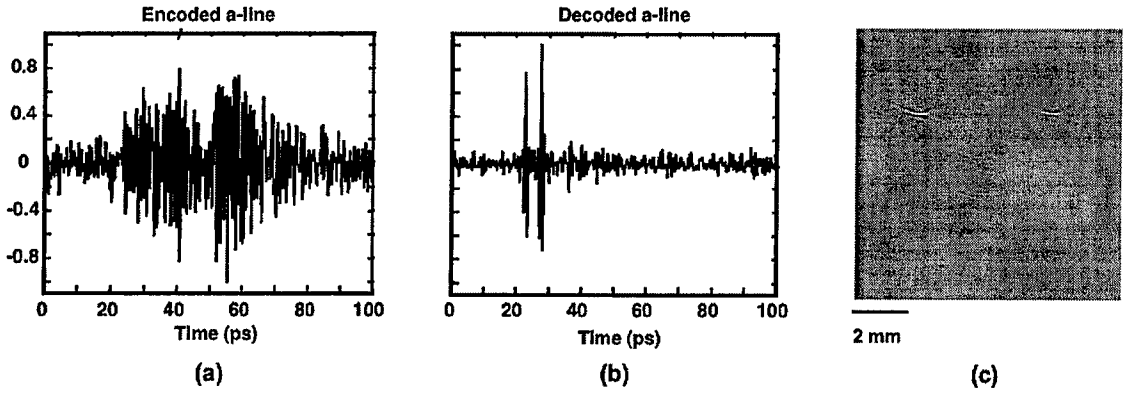

Fig. 14: (a) Encoded waveform. (b) Decoded waveform. (c) Reconstructed image from decoded data set.

AFRL-SR-AR-TR-05-

0236

REPORT DOCUMENTATION PAGE

1. AGENCY USE ONLY (Leave Blank)	2. REPORT DATE 10/4/04 4/15/05	3. REPORT TYPE AND DATES COVERED Final 7/15/02-9/30/04

4. TITLE AND SUBTITLE
Three-Dimensional Terahertz Imaging

5. FUNDING NUMBERS
F49620-02-1-0389

6. AUTHOR(S)
Theodore B. Norris.

7. PERFORMING ORGANIZATION NAME(S) AND ADDRESS(ES)
University of Michgan
2200 Bonisteel Blvd.
Ann Arbor, MI 48109-2099

8. PERFORMING ORGANIZATION REPORT NUMBER

9. SPONSORING / MONITORING AGENCY NAME(S) AND ADDRESS(ES)
U. S. Army Research Office
P.O. Box 12211
Research Triangle Park, NC 27709-2211

10. SPONSORING / MONITORING AGENCY REPORT NUMBER

11. SUPPLEMENTARY NOTES
The views, opinions and/or findings contained in this report are those of the author(s) and should not be construed as an official Department of the Army position, policy or decision, unless so designated by other documentation.

12 a. DISTRIBUTION / AVAILABILITY STATEMENT
Approved for public release; distribution unlimited.

12 b. DISTRIBUTION CODE

13. ABSTRACT (Maximum 200 words)

Three-dimensional imaging has been demonstrated using single-cycle terahertz electromagnetic pulses. Reflection-mode imaging was performed with a photoconductive transmitter and receiver and a reconstruction algorithm based on time reversal. A two-dimensional array was synthesized from ten concentric ring annular arrays with numerical apertures ranging from 0.27 to 0.43. The system clearly distinguished image planes separated by 1.5 mm and achieved a lateral resolution of 1.1 mm. In terms of the illuminating terahertz power spectrum, the lateral resolution was 38% and 81% of the peak and mean wavelengths, respectively. Coded excitation has also been explored to improve the signal-to-noise ratio. A separate imaging system was constructed, where a 53-bit binary waveform is transmitted while the received signals are digitally compressed. Two-dimensional objects have been imaged with a 13 dB improvement in signal-to-noise ratio.

14. SUBJECT TERMS
diffraction tomography, ultrafast optoelectronics, time reversal

15. NUMBER OF PAGES
19

16. PRICE CODE

17. SECURITY CLASSIFICATION OR REPORT	18. SECURITY CLASSIFICATION ON THIS PAGE	19. SECURITY CLASSIFICATION OF ABSTRACT	20. LIMITATION OF ABSTRACT
UNCLASSIFIED	UNCLASSIFIED	UNCLASSIFIED	UL

June 22 05